molecular pharmaceutics

Article

Cite This: *Mol. Pharmaceutics* 2018, 15, 5124−5134

pubs.acs.org/molecularpharmaceutics

P-Glycoprotein (MDR1/ABCB1) Restricts Brain Penetration of the Bruton's Tyrosine Kinase Inhibitor Ibrutinib, While Cytochrome P450-3A (CYP3A) Limits Its Oral Bioavailability

Stéphanie van Hoppe,[†] Johannes J. M. Rood,[‡] Levi Buil,[†] Els Wagenaar,[†] Rolf W. Sparidans,[‡] Jos H. Beijnen,[†,‡] and Alfred H. Schinkel*[,†]

[†]Division of Pharmacology, The Netherlands Cancer Institute, 1066 CX Amsterdam, The Netherlands

[‡]Section of Pharmacoepidemiology & Clinical Pharmacology, Department of Pharmaceutical Sciences, Faculty of Science, Utrecht University, 3512 JE Utrecht, The Netherlands

Supporting Information

ABSTRACT: Ibrutinib (Imbruvica), an oral tyrosine kinase inhibitor (TKI) approved for treatment of B-cell malignancies, irreversibly inhibits the Bruton's tyrosine kinase (BTK). Its abundant metabolite, dihydrodiol-ibrutinib (ibrutinib-DiOH), which is primarily formed by CYP3A, has a 10-fold reduced BTK inhibitory activity. Using in vitro transport assays and genetically modified mouse models, we investigated whether the multidrug efflux transporters ABCB1 and ABCG2 and the multidrug-metabolizing CYP3A enzyme family can affect the oral bioavailability and tissue disposition of ibrutinib and ibrutinib-DiOH. In vitro, ibrutinib was transported moderately by human ABCB1 and mouse Abcg2 but not detectably by human ABCG2. In mice, Abcb1 markedly restricted the brain penetration of ibrutinib and ibrutinib-DiOH, either alone or in combination with Abcg2, resulting in 4.5- and 5.9-fold increases in ibrutinib brain-to-plasma ratios in Abcb1a/1b$^{-/-}$ and Abcb1a/1b;Abcg2$^{-/-}$ mice relative to wild-type mice. Abcb1 and/or Abcg2 did not obviously restrict ibrutinib oral bioavailability, but Cyp3a deficiency increased the ibrutinib plasma AUC by 9.7-fold compared to wild-type mice. This increase was mostly reversed (5.1-fold reduction) by transgenic human CYP3A4 overexpression, with roughly equal contributions of intestinal and hepatic CYP3A4 metabolism. Our results suggest that pharmacological inhibition of ABCB1 during ibrutinib therapy might benefit patients with malignancies or (micro)metastases positioned behind an intact blood-brain barrier, or with substantial expression of this transporter in the malignant cells. Moreover, given the strong in vivo impact of CYP3A, inhibitors or inducers of this enzyme family will likely strongly affect ibrutinib oral bioavailability and, thus, its therapeutic efficacy, as well as its toxicity risks.

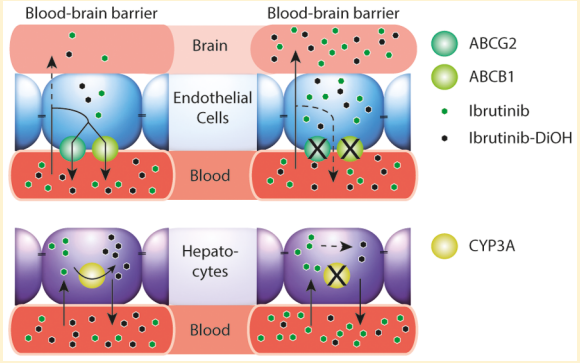

KEYWORDS: *ibrutinib, tyrosine kinase inhibitor, ABCB1, ABCG2, CYP3A4*

INTRODUCTION

Multidrug efflux transporters of the ATP-binding cassette (ABC) protein family affect the disposition of a wide variety of endogenous and exogenous compounds, including numerous anticancer drugs. ABCB1 (P-glycoprotein) and ABCG2 (BCRP) are expressed in the apical membrane of epithelia in a number of organs that are essential for absorption and elimination of drugs, like the small intestine, liver, and kidney.[1−4] They are also abundant in luminal membranes of physiological barriers protecting various sanctuary tissues, such as the blood−brain (BBB), blood−testis, and blood−placenta barriers. At these barriers, penetrating ABCB1 and ABCG2 substrates are immediately pumped out of the epithelial or endothelial cells back into the blood. As a consequence, only small amounts of drug can accumulate in, for instance, the brain. For anticancer drugs, this can compromise treatment of primary brain tumors or (micro)metastases that are present behind a functionally intact BBB.[1−3] Many anticancer drugs, including tyrosine kinase inhibitors (TKIs), are transported substrates of ABCB1, ABCG2, or both. As a result, these transporters can significantly modulate the pharmacokinetic behavior, including plasma levels and tissue distribution, and hence the therapeutic efficacy and toxicity profiles of these drugs.[5] Moreover, when functionally expressed in tumor cells themselves, the transporters can directly contribute to multidrug resistance of the malignancy.

Ibrutinib (Imbruvica, PCI-32765, Figure S1) is an important orally administered TKI currently approved by the FDA and EMA for a number of diseases, including chronic lymphocytic

Received: July 5, 2018
Revised: September 12, 2018
Accepted: September 24, 2018
Published: September 24, 2018

DOI: 10.1021/acs.molpharmaceut.8b00702
Mol. Pharmaceutics 2018, 15, 5124−5134

leukemia, small lymphocytic lymphoma, Waldenström's macroglobulinemia, previously treated mantle cell lymphoma, relapsed/refractory marginal zone lymphoma, and chronic graft versus host disease (cGVHD). The latter application represents the first FDA-approved therapy for this disease.[6] Ibrutinib is an irreversible, covalently binding inhibitor of Bruton's tyrosine kinase (BTK), with promising clinical activity and tolerability in B-cell malignancies and other diseases. Although ibrutinib was initially developed for treatment of B-cell malignancies, recent publications suggest that ibrutinib could additionally be used for the treatment of a range of other malignancies, resulting in an intense interest in this drug.[6−9] Several clinical trials are currently evaluating the efficacy of ibrutinib in metastatic pancreatic adenocarcinoma (NCT02436668), smoldering myeloma (NCT02943473), nonsmall cell lung cancer with an epidermal growth factor receptor (EGFR) mutation (NCT02321540), and refractory/recurrent primary or secondary central nervous system lymphoma (NCT02315326). A number of these malignancies obviously encompass central nervous system (CNS) lesions, including brain metastases. This broader application spectrum is likely, in part, due to ibrutinib specifically inhibiting not only BTK, but also a subset of other kinases, such as GPIb and GPVI, ErbB4/HER4, Blk, Bmx/Etk, Txk, TEC, EGFR, ErbB2/HER2, JAK3, HCK, and ITK.[8,10−13]

Given the high ABCB1 and ABCG2 expression in the BBB, these transporters could potentially limit brain accumulation of ibrutinib, which might reduce the therapeutic efficacy against CNS lesions, including brain (micro)metastases. However, the current FDA and EMA documentation for this drug states that in vitro studies suggest that ABCB1 and ABCG2 do not transport ibrutinib, although they might be inhibited by ibrutinib at clinical doses.[6] A recent study further reported that ibrutinib can stimulate hABCB1-mediated ATPase activity.[14] It was therefore of interest to study these interactions in more detail.

The absolute oral bioavailability of ibrutinib in patients is low (around 3−8%), and this is likely due in part to extensive first-pass metabolism, primarily by cytochrome-P450 (CYP) 3A. Its main metabolite, dihydrodiol-ibrutinib (DiOH, PCI-45227, Figure S1), has an inhibitory activity toward BTK approximately 10−15 times lower than that of the parent compound.[6] Ibrutinib-DiOH, which is thus modestly pharmacodynamically active, is formed through epoxidation and subsequent oxidation of the reactive acrylamide group.[15] Ibrutinib is mainly excreted via feces after phase I and II biotransformation. In humans, CYP3A4 is also the predominant CYP isoenzyme involved in the biotransformation of a range of other TKIs, such as imatinib, nilotinib, bosutinib, dasatinib, and ponatinib.[16−20]

In the present study, we investigated whether ibrutinib is a transported substrate of ABCB1 and ABCG2 in vitro and in vivo, and how this might affect the oral plasma pharmacokinetics and tissue distribution, including brain penetration, of ibrutinib and ibrutinib-DiOH in appropriate knockout mouse models. Furthermore, the substantial metabolism of ibrutinib by CYP3A[6] means that induction or inhibition of this enzyme complex may dramatically influence ibrutinib exposure. We therefore also studied the in vivo tissue-specific influence of CYP3A on the oral systemic availability and tissue exposure of ibrutinib and ibrutinib-DiOH in Cyp3a knockout and humanized transgenic mouse models.

MATERIALS AND METHODS

Chemicals. Ibrutinib (>99%) was purchased from Alsachim (Illkirch Graffenstaden, France), zosuquidar was obtained from Sequoia Research Products (Pangbourne, U.K.), and Ko143 was from Tocris Bioscience (Bristol, U.K.). Isoflurane was purchased from Pharmachemie (Haarlem, The Netherlands), heparin (5000 IU ml^{-1}) was from Leo Pharma (Breda, The Netherlands), and bovine serum albumin (BSA) fraction V was from Roche (Mannheim, Germany). All chemicals used in the chromatographic ibrutinib assay were described before.[21]

Transport Assays. Polarized Madin−Darby canine kidney (MDCK-II) cell lines transduced with either human (h)-ABCB1, murine (m)Abcg2, or (h)ABCG2 cDNA were cultured and used as described previously.[22] Transepithelial transport assays were performed in triplicate on 12-well microporous polycarbonate membrane filters (3.0-μm pore size, Transwell 3402, Corning Inc., Lowell, MA), as described.[22] In short, cells were allowed to grow to an intact monolayer in 3 days, which was monitored with transepithelial electrical resistance (TEER) measurements. On the third day, cells were pre-incubated with the relevant inhibitors for 1 h, where 5 μM zosuquidar (ABCB1 inhibitor) and/or 5 μM Ko143 (ABCG2/Abcg2 inhibitor) were added to both apical and basolateral compartments. To inhibit endogenous canine ABCB1 when testing the MDCK-II Abcg2 and MDCK-II ABCG2 cell lines, we added 5 μM zosuquidar (ABCB1 inhibitor) to the culture medium throughout the experiment. The experiment was initiated by replacing the incubation medium from the donor compartment with freshly prepared medium containing 2 μM ibrutinib alone or in combination with the appropriate inhibitors. At 1, 2, 4, and 8 h, 50-μL samples were collected from the acceptor compartment and stored at −30 °C until analysis. The amount of transported drug was calculated after correction for volume loss due to sampling at each time point. Active transport was expressed by the transport ratio (r), which is defined as the amount of apically directed transport divided by the amount of basolaterally directed translocation at a defined time point.

Animals. Female wild-type (WT), Abcb1a/1b$^{-/-}$,[23] Abcg2$^{-/-}$,[24] Abcb1a/1b;Abcg2$^{-/-}$,[25] Cyp3a$^{-/-}$, hCyp3aXA, hCyp3aXV, and hCyp3aXAV mice,[26] all of a >99% FVB strain background, were used. Mice between 9 and 14 weeks of age were used in groups of 5−6 mice per strain. The mice were kept in a temperature-controlled environment with a 12 h light/dark cycle and received a standard diet (AM-II, Hope Farms, Woerden, The Netherlands) and acidified water ad libitum. Animals were housed and handled according to institutional guidelines in compliance with Dutch and EU legislation.

Drug Solutions. Ibrutinib was dissolved at a concentration of 24.4 mg/mL in DMSO, polysorbate 80, and ethanol (final solvent ratios 1:20:20 (v/v/v)). It was then further diluted with 5% (w/v) glucose in water to obtain a 1 mg/mL ibrutinib solution in water containing 0.1% DMSO, 2% (v/v) polysorbate 80, 2% (v/v) ethanol, and 4.795% (w/v) glucose. Ibrutinib was administered orally at a dose of 10 mg/kg (10 μL/g).

Plasma and Tissue Pharmacokinetics of Ibrutinib. To minimize variation in absorption, mice were fasted for 3 h prior to the oral administration of ibrutinib using a blunt-ended needle. The 50-μL blood samples were drawn from the tail

DOI: 10.1021/acs.molpharmaceut.8b00702
Mol. Pharmaceutics 2018, 15, 5124−5134

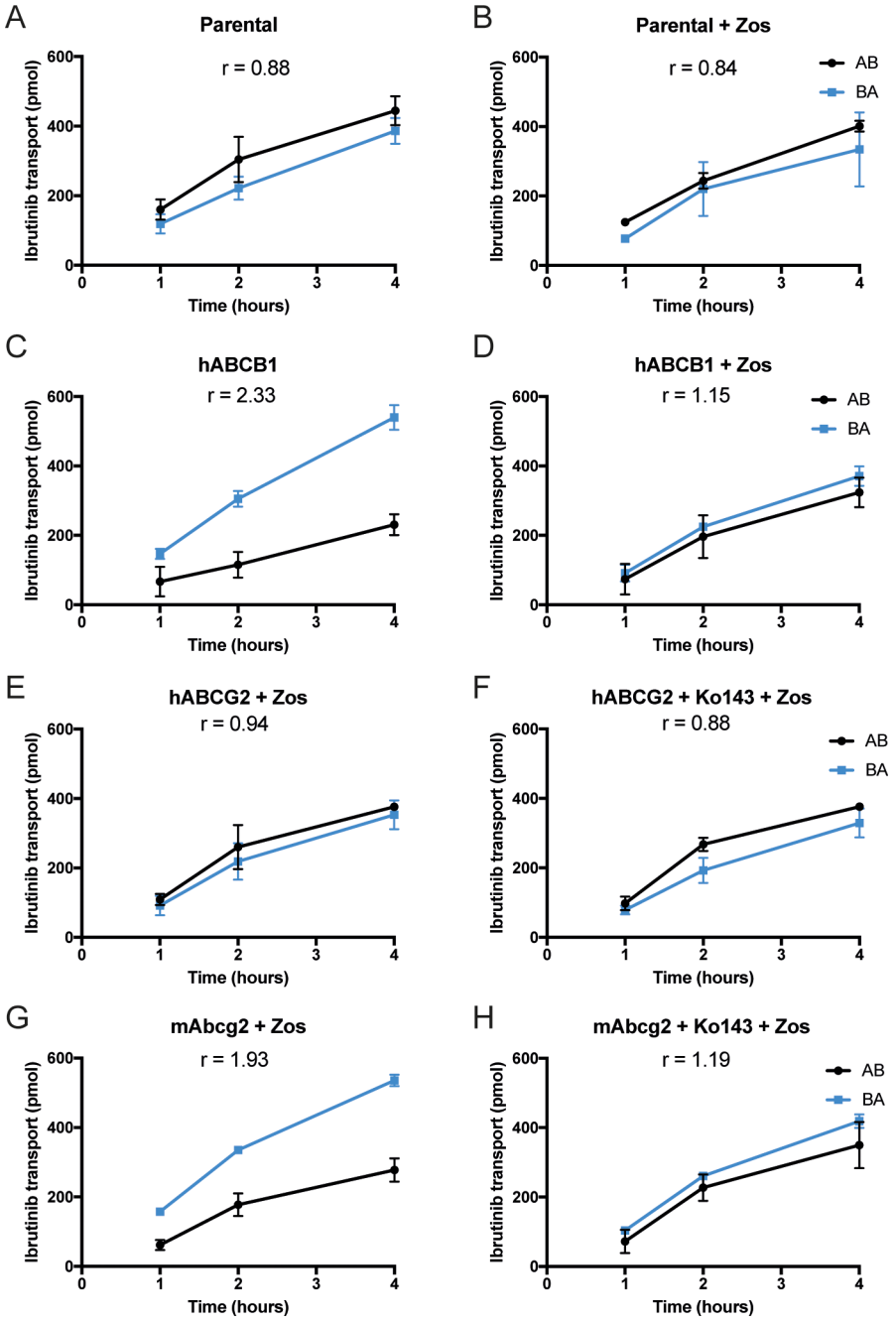

Figure 1. In vitro transport of ibrutinib. Transepithelial transport of ibrutinib (2 μM) was assessed in MDCK-II cells either nontransduced (A, B) or transduced with hABCB1 (C, D), mAbcg2 (E, F), or hABCG2 (G, H) cDNA. At t = 0 h, ibrutinib was added to the donor compartment; thereafter, at t = 1, 2, and 4 h, the concentrations were measured and plotted as the total amount (pmol) of translocated drug (n = 3). (B, D−H) Zosuquidar (Zos, 5 μM) or Ko143 (5 μM) were added as indicated to inhibit hABCB1 or hABCG2 and mAbcg2, respectively. r, relative transport ratio at 4 h. BA (blue squares) translocation from the basolateral to the apical compartment; AB (black circles), translocation from the apical to the basolateral compartment. Data are presented as mean ± SD.

vein using heparin-coated capillaries (Sarstedt, Germany). At the last time point, mice were anesthetized using isoflurane inhalation, and blood was collected via cardiac puncture. For the 8-h experiment, tail vein sampling took place at 0.25, 0.5, 1, 2, and 4 h after oral administration; for the 1-h experiment, tail vein sampling took place at 5, 10, 15, and 30 min after oral administration; and finally for the 20 min experiment, tail vein sampling took place at 5, 10, and 15 min after oral administration. At the end point, mice were sacrificed by cervical dislocation and a set of organs was rapidly removed, weighed, and subsequently frozen as whole organs at −30 °C. Organs were allowed to thaw on ice and homogenized in appropriate volumes of 4% (w/v) BSA in water using a FastPrep-24 device (MP Biomedicals, SA, California, USA). Homogenates were stored at −30 °C until analysis. Blood samples were immediately centrifuged at 9000 × g for 6 min at 4 °C, and plasma was collected and stored at −30 °C until analysis. Ibrutinib concentrations in brain tissue were corrected for the amount of plasma present in the vascular space (∼1.4%).[27]

DOI: 10.1021/acs.molpharmaceut.8b00702
Mol. Pharmaceutics 2018, 15, 5124−5134

Table 1. Pharmacokinetic Parameters of Ibrutinib at 8 and 1 h after Oral Administration of 10 mg/kg Ibrutinib to Female WT, Abcb1a/1b$^{-/-}$, Abcg2$^{-/-}$, and Abcb1a/1b;Abcg2$^{-/-}$ Mice[a]

		genotype			
parameter	time (h)	WT	Abcb1a/1b$^{-/-}$	Abcg2$^{-/-}$	Abcb1a/1b;Abcg2$^{-/-}$
AUC_{0-8} (h.ng/mL)	8	431 ± 97			404 ± 78
C_{max} (ng/mL)		609 ± 276			837 ± 131
T_{max} (min)		7 ± 4			5 ± 0
AUC_{0-1} (h.ng/mL)	1	340 ± 59	190 ± 69***	350 ± 34###	169 ± 31***
C_{max} (ng/mL)		748 ± 93	455 ± 164	751 ± 95	372 ± 107
T_{max} (min)		≤5	≤5	7 ± 3	6 ± 2
C_{brain} (ng/g)		8.93 ± 4.58	18.3 ± 9.86	9.41 ± 1.86##	25.9 ± 10.4**
brain-to-plasma ratio		0.081 ± 0.015	0.366 ± 0.086***	0.084 ± 0.007###	0.481 ± 0.074***
fold change		1	4.5	1	5.9
C_{liver} (ng/g)		162 ± 76	54.3 ± 23	152 ± 37	77 ± 24
liver-to-plasma ratio		1.49 ± 0.10	1.39 ± 0.25	1.36 ± 0.19	1.50 ± 0.21
fold change		1	0.9	0.9	1

[a]AUC, area under the plasma concentration−time curve; C_{max}, maximum ibrutinib concentration in plasma; T_{max}, the time (min) after drug administration needed to reach maximum plasma concentration; C_{brain}, brain concentration; C_{liver}, liver concentration. *, $p < 0.05$; **, $p < 0.01$; and ***, $p < 0.001$ compared to WT mice and #, $p < 0.05$; ##, $p < 0.01$; and ###, $p < 0.001$ compared to Abcb1a/1b;Abcg2$^{-/-}$ mice. Data are given as mean ± SD.

Drug Analysis. Ibrutinib and ibrutinib-DiOH concentrations in culture medium, plasma, and tissue homogenates were analyzed with a previously reported liquid-chromatography tandem mass spectrometric (LC-MS/MS) assay using deuterated internal standards.[21]

Statistics and Pharmacokinetic Calculations. The unpaired two-tailed Student's t test was used to determine the significance of differences in the transepithelial transport assays. The area under the curve (AUC) of the plasma concentration−time curve was calculated using the trapezoidal rule, without extrapolating to infinity. Individual concentration−time data were used to determine the peak plasma concentration (C_{max}) and the time to reach C_{max} (T_{max}). Ordinary one-way analysis of variance (ANOVA) was used to determine significant differences between groups. Post hoc Tukey's multiple comparisons were used to compare significant differences between individual groups. When variances were not homogeneously distributed, data were log-transformed before applying statistical tests. Differences were considered statistically significant when $p < 0.05$. Data are presented as mean ± SD, with each experimental group containing 5−6 mice.

RESULTS

We first studied the interaction between ibrutinib and ABCB1 and ABCG2 in vitro by measuring ibrutinib (2 μM) translocation through polarized monolayers of the MDCKII parental cell line and subclones transduced with human hABCB1, hABCG2, or mouse mAbcg2 cDNA. As shown in Figure 1A, we observed no net apically directed ibrutinib transport in the parental cell line (transport ratio $r = 0.88$). This was not significantly altered when the cells were treated with the ABCB1 inhibitor zosuquidar ($r = 0.84$, Figure 1B), suggesting that there is virtually no background transport mediated by the endogenous canine ABCB1 present in the MDCKII cells.[28] In MDCKII cells transduced with human ABCB1, we observed active apically directed transport with $r = 2.33$, which was almost completely blocked by zosuquidar, indicating that ibrutinib is a transport substrate for hABCB1 (Figure 1C,D). In subsequent transport experiments using MDCKII cells expressing human or mouse ABCG2, zosuquidar was included to block any background transport mediated by endogenous canine ABCB1. We observed substantial apically directed transport by mAbcg2 ($r = 1.93$), whereas no transport was detected for hABCG2 ($r = 0.94$), as shown in Figure 1E−H. Ibrutinib transport by mAbcg2 was efficiently blocked by the ABCG2 inhibitor Ko143. Ibrutinib thus appears to be transported by hABCB1 and mAbcg2 but, at this concentration, not noticeably by hABCG2.

On the basis of these transport data, we studied the single and combined effects of Abcb1 and Abcg2 on the plasma and tissue pharmacokinetics of ibrutinib and its pharmacodynamically active metabolite, ibrutinib-DiOH, using WT, Abcb1a/1b$^{-/-}$, Abcg2$^{-/-}$, and Abcb1a/1b;Abcg2$^{-/-}$ mice. Because ibrutinib is taken orally by patients, we administered ibrutinib orally at a dose of 10 mg/kg, roughly physiologically equivalent to the lower end of the human recommended dosages (140 mg/day). In a pilot experiment, we analyzed the plasma concentrations of ibrutinib and ibrutinib-DiOH over 8 h in WT and Abcb1a/1b;Abcg2$^{-/-}$ mice. In this experiment, performed in our old mouse facility, we found no significant differences in the $AUC_{0-8\ h}$ values between the WT and knockout mice (Figure S2A,B; Table 1). Ibrutinib was very rapidly absorbed, with a T_{max} occurring before 5 min, and also quite rapidly cleared. Within 15 min, ibrutinib-DiOH concentrations were substantially higher than those of the parent drug, reaching a T_{max} around 15−30 min, and with ibrutinib-DiOH/ibrutinib ratios staying well over a factor of 5 from 30 min on to at least 3 h after administration (Figure S3, Table S1). A subsequent 1-h experiment including all four ABC transporter mouse strains was performed more than a year later, after transfer of these strains to our new mouse facility. This transfer included a full cleanup by hysterectomy and a complete changeover in the microflora to that of another commercial animal supplier. Possibly related to this changeover, we observed that, under these circumstances, the plasma AUC of ibrutinib in Abcb1a/1b;Abcg2$^{-/-}$ as well as Abcb1a/1b$^{-/-}$ mice was almost 2-fold lower than that in WT mice, whereas Abcg2$^{-/-}$ mice behaved more or less like WT mice (Figure 2A, Table 1). In other respects, however, the plasma pharmacokinetics in WT mice of both ibrutinib and ibrutinib-DiOH were very similar to those seen in the pilot experiment,

DOI: 10.1021/acs.molpharmaceut.8b00702
Mol. Pharmaceutics 2018, 15, 5124−5134

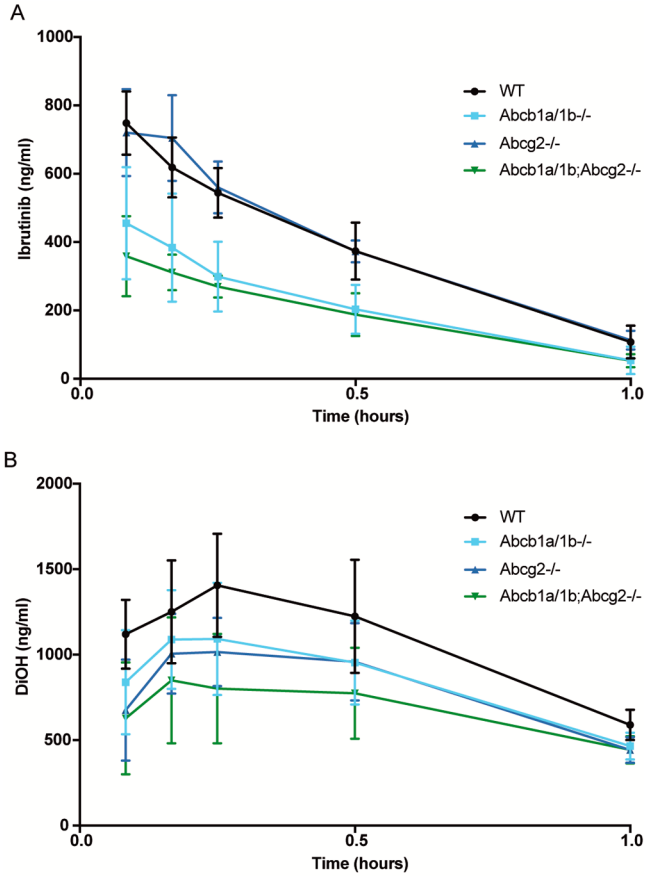

Figure 2. Plasma concentration−time curves of ibrutinib (A) and ibrutinib-DiOH (DiOH) (B) in female WT (black circles), Abcb1a/1b$^{-/-}$ (blue squares), Abcg2$^{-/-}$ (dark blue triangles), and Abcb1a/1b;Abcg2$^{-/-}$ (green triangles) mice over 1 h after oral administration of 10 mg/kg ibrutinib. Note the difference in the *Y*-axis scales between the panels. Data are given as mean ± SD, n = 5−6 mice per group.

with rapid absorption of ibrutinib (T_{max} before 5 min), a T_{max} of ibrutinib-DiOH around 15 min (Figure 2B, Table S1), and a ibrutinib-DiOH/ibrutinib ratio rising above a factor of 5 well within 1 h (Figure S4). The $AUC_{0-1\ h}$ for ibrutinib in WT mice was also very similar for both experiments (274 and 340 h.ng/mL, respectively). Although there was a tendency for the ibrutinib-DiOH/ibrutinib ratio to be higher in the Abcb1a/1b;Abcg2$^{-/-}$ as well as the Abcb1a/1b$^{-/-}$ mice compared to the WT mice, this did not reach statistical significance (Figure S4). Abcg2$^{-/-}$ mice behaved generally similar to WT mice in this respect. Thus, apart from the impact of Abcb1 deficiency, which resulted in ∼2-fold lower plasma levels of ibrutinib in the second, but not the first, experiment, there does not seem to be a major impact of Abcb1 and/or Abcg2 on ibrutinib to ibrutinib-DiOH conversion.

To investigate the impact of single and combined knockout of Abcb1a/1b and Abcg2 on ibrutinib brain distribution, we isolated mouse tissues (brain, liver, kidneys, and spleen) at the end of the 1 h pharmacokinetic experiment. Figure 3A shows that ibrutinib accumulated to a low extent in the brain of WT and Abcg2$^{-/-}$ mice but more highly in Abcb1a/1b$^{-/-}$ and Abcb1a/1b;Abcg2$^{-/-}$ mice. Correction for the substantial differences in plasma concentration at 1 h and the plasma AUCs showed that brain-to-plasma ratios and brain accumulation of ibrutinib were markedly (and highly significantly) increased in both the Abcb1-deficient strains but not in the single Abcg2-deficient strain (Figure 3B,C). In contrast, analysis of the liver, which often equilibrates rapidly with drug levels in plasma, yielded no significant differences in the liver-to-plasma ratio or liver accumulation (Figure 3D−F). Together, these data indicate that Abcb1a/1b markedly restricts brain accumulation of ibrutinib. Whether Abcg2 also contributes to this process is uncertain, as the (modest) differences between the Abcb1a/1b$^{-/-}$ and Abcb1a/1b;Abcg2$^{-/-}$ brains were not statistically significant (Figure 3B,C). The intrinsic brain accumulation of ibrutinib was quite low in WT mice, with a brain-to-plasma ratio of 0.081, which rose to about 0.37−0.48 in the Abcb1a/1b$^{-/-}$ or the combination Abcb1a/1b;Abcg2$^{-/-}$ strain, respectively (Figure 3B, Table 1). Compared to a liver-to-plasma ratio of 1.4−1.5 at this time point (Figure 3E), this suggests a fairly good brain penetration of this drug but only when Abcb1a/1b is absent.

Ibrutinib-DiOH is substantially more polar than the parent ibrutinib, and this is probably reflected in the lower brain-to-plasma ratios and brain accumulation than for ibrutinib (Figure 4A−C). However, the impact of the absence of Abcb1a/1b on altering brain-to-plasma ratios and brain accumulation of ibrutinib-DiOH was even more pronounced than for ibrutinib, with 12- to 15-fold increases relative to wild-type values (Figure 4A−C, Table S1). Like for ibrutinib, any contribution of Abcg2 to limiting ibrutinib-DiOH brain accumulation was at best small. At the same time, the relative liver accumulation of ibrutinib-DiOH was very similar to that of ibrutinib, and not significantly different between the tested mouse strains (Figure 4D−F). Similar parameters for the distribution of both ibrutinib and ibrutinib-DiOH to the kidney and spleen also did not yield pronounced differences between the strains, although there may be some impact of Abcb1a/1b deficiency on increasing ibrutinib spleen distribution (Figures S5 and S6). Distribution of both ibrutinib and ibrutinib-DiOH to the brain thus appears to be markedly limited by Abcb1a/1b activity, but distribution to most of the other tested organs is not. In spite of the marked changes in brain distribution of ibrutinib, we did not see any indications for the toxicity of ibrutinib at the dosages used in the Abcb1a/1b;Abcg2$^{-/-}$ mice.

CYP3A is thought to primarily mediate the oxidation of ibrutinib to ibrutinib-DiOH, and we therefore also investigated the extent and tissue specificity of the impact of CYP3A in WT, Cyp3a$^{-/-}$, Cyp3aXA, Cyp3aXV, and Cyp3aXAV mice. Cyp3a$^{-/-}$ mice lack all mouse Cyp3a proteins, whereas the "humanized" Cyp3aXA, Cyp3aXV, and Cyp3aXAV strains express human CYP3A4 in, respectively, the liver (XA), the intestine (XV), or in both liver and intestine (XAV) of the Cyp3a$^{-/-}$ mice. We first performed a pilot study with oral ibrutinib at 10 mg/kg in WT, Cyp3a$^{-/-}$, and Cyp3aXAV mice, analyzing the ibrutinib and ibrutinib-DiOH plasma concentrations over 8 h. We found that the absence of Cyp3a led to highly increased ibrutinib concentrations in the plasma compared to WT mice, resulting in a 9.7-fold increased $AUC_{0-8\ h}$, whereas the T_{max} was not substantially altered (Figure 5A, Table 2). Conversely, the formation of ibrutinib-DiOH was dramatically decreased in Cyp3a$^{-/-}$ mice, resulting in only 6.7% of the ibrutinib-DiOH $AUC_{0-8\ h}$ in WT mice (Figure 5C, Table S2). These data indicate that the mouse Cyp3a proteins are a major factor in metabolizing ibrutinib to ibrutinib-DiOH. When transgenic human CYP3A4 was expressed in both the livers and intestines of Cyp3a$^{-/-}$ mice (Cyp3aXAV), the ibrutinib plasma concentrations decreased

DOI: 10.1021/acs.molpharmaceut.8b00702
Mol. Pharmaceutics 2018, 15, 5124−5134

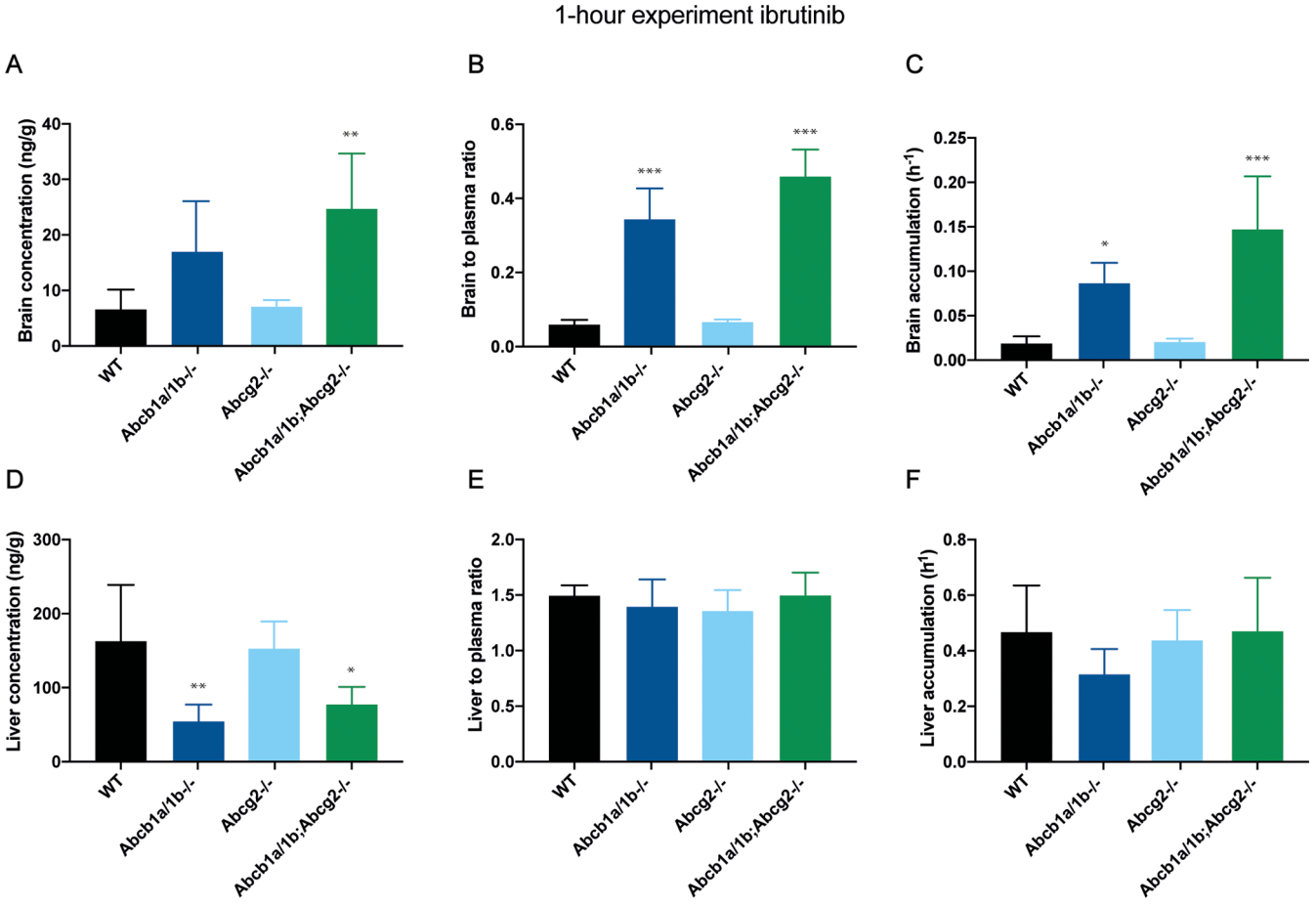

Figure 3. Brain and liver concentration (A, D), tissue-to-plasma ratio (B, E), and relative tissue accumulation (C, F) of ibrutinib in female WT, Abcb1a/1b$^{-/-}$, Abcg2$^{-/-}$, and Abcb1a/1b;Abcg2$^{-/-}$ mice 1 h after oral administration of 10 mg/kg ibrutinib. *, $p < 0.05$; **, $p < 0.01$; and ***, $p < 0.001$ compared to WT mice. Data are given as mean ± SD, n = 5−6 mice per group.

again by 5-fold to less than 2-fold the $AUC_{0-8\ h}$ in WT mice (Figure 5A, Table 2). At the same time, plasma levels of ibrutinib-DiOH in Cyp3aXAV mice increased by 4.2-fold compared to Cyp3a$^{-/-}$ mice, to about 28% of the ibrutinib-DiOH $AUC_{0-8\ h}$ seen in WT mice (Figure 5C, Table S2. These data indicate a substantial, albeit not complete, reversal of ibrutinib to ibrutinib-DiOH conversion by transgenic human CYP3A4 expression in the liver and intestine. Thus, the combined endogenous mouse Cyp3a proteins have a higher overall capacity to metabolize ibrutinib to ibrutinib-DiOH than the exogenously (but orthotopically) expressed human CYP3A4. Accordingly, when we plotted the plasma ibrutinib-DiOH to ibrutinib concentration ratio over the first 3 h, the high ratio observed in WT mice (rising well above 5 within 30 min) was very low in Cyp3a$^{-/-}$ mice (0.04 around 30 min), but only returned to a ratio of around 1 at 30 min in the Cyp3aXAV mice (Figure S7). A small 1-h follow-up experiment in WT and Cyp3a$^{-/-}$ mice revealed very similar profiles (Figure S8).

To further analyze the separate and combined in vivo impact of hepatic and intestinal CYP3A4 on ibrutinib to ibrutinib-DiOH metabolism around or shortly after the T_{max} of ibrutinib, we performed a short-term (20 min) oral pharmacokinetic experiment in WT, Cyp3a$^{-/-}$, Cyp3aXA, Cyp3aXV, and Cyp3aXAV mice. As shown in Figure 5B,D, the interindividual variation in plasma levels was high, especially in WT mice, which is not uncommon shortly after oral drug administration. Nonetheless, absence of Cyp3a led to a highly significant, 8.7-fold, increase in ibrutinib plasma levels ($AUC_{0-0.33\ h}$), which was partly reversed by either hepatic CYP3A4 expression (2.3-fold reversal) or intestinal CYP3A4 expression (2.7-fold reversal). Combined hepatic and intestinal CYP3A4 expression had an additive effect, resulting in a 5.1-fold reversal of ibrutinib plasma levels (Figure 5B, Table 2). Also, over this time period, reversal by the transgenic human CYP3A4 was therefore extensive but not completely back to WT levels. The changes in ibrutinib-DiOH plasma levels between the strains mirrored the changes in levels of ibrutinib metabolism, with absence of Cyp3a resulting in a 12.4-fold decrease in ibrutinib-DiOH levels ($AUC_{0-0.33\ h}$), hepatic and intestinal CYP3A4 expression causing a 4.4- and 6.5-fold reversal, respectively, and the combination expression causing a 7.9-fold reversal (Figure 5D, Table S2). Plotting the plasma ibrutinib-DiOH-to-ibrutinib concentration ratios confirmed these separate and additive effects (Figure S9E), including that the reversal even in the Cyp3aXAV strain was far from completely back to the WT levels. Collectively, the data indicate that, in these mouse strains, hepatic and intestinal CYP3A4 have a more or less comparable impact on reducing oral ibrutinib plasma levels by metabolizing it to ibrutinib-DiOH. Detailed analysis of changes in the tissue levels of ibrutinib and ibrutinib-DiOH was hampered by the high interindividual variation at this early time point, but the ibrutinib-DiOH-to-ibrutinib ratios in all tested tissues (liver, kidney, and spleen) generally reflected

DOI: 10.1021/acs.molpharmaceut.8b00702
Mol. Pharmaceutics 2018, 15, 5124−5134

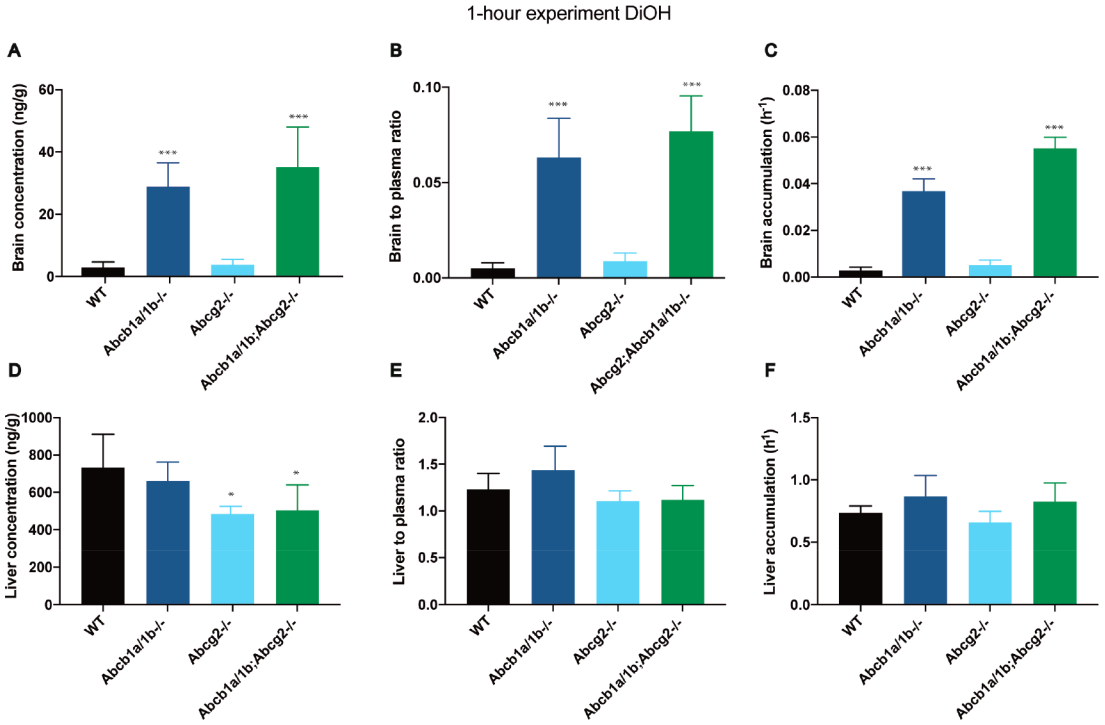

Figure 4. Brain and liver concentration (A, D), tissue-to-plasma ratio (B, E), and relative tissue accumulation (C, F) of ibrutinib-DiOH (DiOH) in female WT, Abcb1a/1b$^{-/-}$, Abcg2$^{-/-}$, and Abcb1a/1b;Abcg2$^{-/-}$ mice 1 h after oral administration of 10 mg/kg ibrutinib. *, $p < 0.05$; **, $p < 0.01$; and ***, $p < 0.001$ compared to WT mice. Data are given as mean ± SD, $n = 5–6$ mice per group.

those seen in plasma (Figure S9A–E), indicating a relatively rapid equilibration of both compounds between these tissues and plasma.

DISCUSSION

Our results show that ibrutinib is modestly transported in vitro by human ABCB1 and mouse Abcg2, but not detectably by human ABCG2. In in vivo mouse models, mAbcb1 and mAbcg2 do not appear to restrict the oral bioavailability of ibrutinib, although under some circumstances, mAbcb1 deficiency may indirectly reduce ibrutinib availability (see below). However, the brain distribution of ibrutinib is markedly restricted by mAbcb1 in the BBB, but not substantially by mAbcg2, even in the absence of mAbcb1 activity. The brain distribution of ibrutinib-DiOH, the primary active metabolite of ibrutinib, is also strongly limited by mAbcb1 activity. In contrast, the distribution of ibrutinib and ibrutinib-DiOH to other major tissues, such as liver, kidney, and spleen, is not markedly affected by mAbcb1 and/or mAbcg2 activity, with the possible exception of a small effect of Abcb1a/1b deficiency in ibrutinib spleen distribution. No ibrutinib toxicity was observed in the Abcb1a/1b;Abcg2-deficient mice. We further found that mouse Cyp3a deficiency caused a profound increase in ibrutinib plasma levels, apparently due to reduced conversion of ibrutinib to ibrutinib-DiOH. Overexpression of human CYP3A4 in either liver or intestine of Cyp3a$^{-/-}$ mice markedly reduced ibrutinib oral bioavailability, and to roughly similar extents. The concomitant ibrutinib-DiOH levels observed in these strains qualitatively reflected the predicted changes in conversion of ibrutinib to ibrutinib-DiOH by Cyp3a and CYP3A4.

Our in vitro transport data contrast with the FDA and EMA documentation on ibrutinib, stating that in vitro studies suggest that ABCB1 and ABCG2 do not transport ibrutinib.[6,29] Instead, we found clear transport of ibrutinib by hABCB1 and mAbcg2, with efflux ratios (2.33, 1.93) well above the often-used cutoff value of 1.5, and they were fully inhibitable with specific ABCB1 and ABCG2 inhibitors. We attribute this apparent discrepancy to the relative sensitivity of the transepithelial transport assays applied by us. The in vivo significance of these findings is further supported by the marked effect of mAbcb1 deficiency on the brain distribution of ibrutinib (Figure 3, Table 1). mAbcg2, instead, did not appear to have a marked impact in restricting brain accumulation of ibrutinib. It is possible that ABCB1 in humans will also limit brain distribution of ibrutinib, which could affect the therapeutic efficacy of this drug against brain malignancies, either primary lesions or (micro)metastases, that are positioned in whole or in part behind a functional BBB. However, quantitative proteomic research has demonstrated that humans possess an ∼4-fold more abundant BBB expression of ABCG2 relative to ABCB1 compared to mice.[35] It can therefore not be excluded that, in humans, there may still be a role of ABCG2 in limiting ibrutinib brain distribution, even though we did not find a clear impact of Abcg2 in the mouse BBB. Conversely, as the human BBB ABCB1 expression is 2.3-fold lower than that of the mouse BBB Abcb1a, the impact of ABCB1 in human brain penetration of ibrutinib might be somewhat smaller than that in mice.

It is worth noting, that the intrinsic brain distribution of ibrutinib is not very low, with brain-to-plasma ratios of 8% in WT mice, increasing to 37–48% in the absence of Abcb1 and Abcg2 (Table 1). Even though most of the primary malignancies (lymphomas) for which ibrutinib is currently prescribed do not often occur in, or metastasize to, the brain, this does happen now and then. For instance, in Bing Neel syndrome, malignant lymphoplasmacytic cells from Walden-

DOI: 10.1021/acs.molpharmaceut.8b00702
Mol. Pharmaceutics 2018, 15, 5124–5134

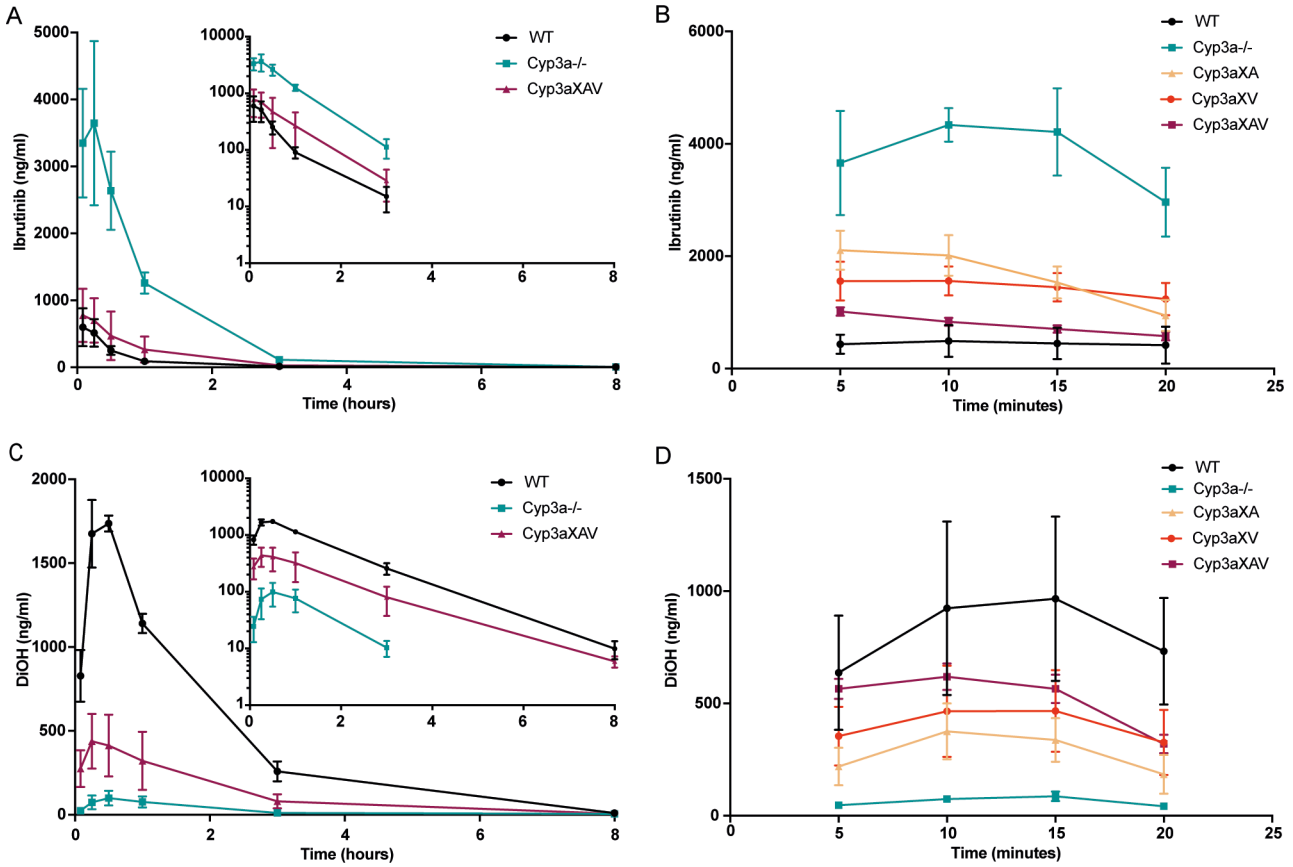

Figure 5. Plasma concentration−time curves of ibrutinib (A, B) and ibrutinib-DiOH (DiOH) (C, D) in female WT (black circles), Cyp3a$^{-/-}$ (blue squares), Cyp3aXA (peach triangles), Cyp3aXV (red circles), and Cyp3aXAV (maroon triangles) mice over 8 h (A, C) or 20 min (B, D) after oral administration of 10 mg/kg ibrutinib. (Insets) Semilog plots of the data. When the 8 h data were below the lower limit of quantification, data were only plotted up until 3 h. Note the different concentration scales in panels A and C as well as panels B and D. Data are given as mean ± SD, n = 5−6 mice per group.

ström's macroglobulinemia infiltrate the CNS, mantle cell lymphoma can disseminate to the CNS, and primary CNS lymphoma also occurs.[30−34] Interestingly, ibrutinib is already considered a potential treatment option for all of these disorders, as its intrinsic brain penetration is thought to be fair based on CSF drug levels.[33] Moreover, brain metastases are common for a number of malignancies, including nonsmall cell lung cancer, for which ibrutinib is currently in clinical trials. Considering the broad interest in applying ibrutinib to a range of other cancers as well, this will further increase the likelihood of BBB function interfering with optimal therapeutic efficacy of this drug. Moreover, the observation that hABCB1 can actively extrude ibrutinib opens up the possibility that, when substantially expressed in lymphoma or tumor cells themselves (as is often the case[36,37]), it can significantly contribute directly to resistance against this drug, which acts against an intracellular target. Given these considerations, it might be worthwhile to consider administering ibrutinib together with a strong ABCB1 inhibitor under some circumstances in order to increase efficacy against brain lesions and malignancies resistant due to ABCB1 overexpression.

From our data, ibrutinib-DiOH also appears to be a transported substrate of Abcb1 in vivo, which is in line with EMA documentation mentioning in vitro transport by hABCB1.[29] While its brain distribution is strongly restricted by mAbcb1 (Figure S5 and Table S1), the absolute brain distribution of ibrutinib-DiOH relative to ibrutinib is still very low, even in Abcb1-deficient mice (brain-to-plasma ratio of ∼7%). Since ibrutinib-DiOH is also much less (10/15-fold) pharmacodynamically active than ibrutinib, it seems very unlikely that it would substantially contribute to the therapeutic efficacy against CNS lesions.

The oral bioavailability of ibrutinib is clearly not restricted by mAbcb1 and mAbcg2 activity. This contrasts with the clear impact of mAbcb1 on the brain accumulation of ibrutinib. We (and others) have observed this for a range of different drugs: generally, when a drug is only moderately transported in vitro by ABCB1 and/or ABCG2, such as ponatinib and regorafenib, we see a more pronounced effect of these transporters in restricting the brain accumulation of these drugs than in reducing their oral availability.[38,39] Only when drugs are very efficiently transported substrates, such as afatinib, we tend to see a clear role in oral availability.[4] Whereas the exact reason for this apparent discrepancy is unknown, it may be due to the presence of more broad-specificity uptake systems as well as a higher influx capacity in the intestine as compared to the much more restrictive BBB. An obvious translational implication of these findings is that, when inhibiting ABCB1 and/or ABCG2 with a pharmacological ABCB1/ABCG2 inhibitor, the oral availability of a drug will generally be (much) less enhanced than its brain penetration. Especially when there are potential toxic side effects of higher systemic exposure of the drug(s), this might be an advantage.

DOI: 10.1021/acs.molpharmaceut.8b00702
Mol. Pharmaceutics 2018, 15, 5124−5134

Table 2. Pharmacokinetic Parameters of Ibrutinib at 8 h, 1 h, and 20 min after Oral Administration of 10 mg/kg Ibrutinib to Female WT, Cyp3a$^{-/-}$, Cyp3aXA, Cyp3aXV, and Cyp3aXAV Mice[a]

		genotype				
parameter	time	WT	Cyp3a$^{-/-}$	Cyp3aXA	Cyp3aXV	Cyp3aXAV
AUC_{0-8} (h.ng/mL)	8 h	431 ± 96.6	4166 ± 317***			832 ± 521$^{\#\#\#}$
C_{max} (ng/mL)		609 ± 276	3865 ± 932			798 ± 404
T_{max} (min)		7 ± 4	15 ± 8			9 ± 5
AUC_{0-1} (h.ng/mL)	1 h	341 ± 59	1973 ± 670***			
C_{max} (ng/mL)		748 ± 93	3305 ± 1425			
T_{max} (min)		≤5	13 ± 8			
C_{brain} (ng/g)		8.93 ± 4.58	111 ± 34.7***			
brain-to-plasma ratio		0.081 ± 0.015	0.109 ± 0.021			
fold change		1	1.3			
C_{liver} (ng/g)		162.6 ± 76.4	1415 ± 409 ***			
liver-to-plasma ratio		1.49 ± 0.10	1.38 ± 0.22			
fold change		1	0.9			
$AUC_{0-0.33}$ (h.ng/mL)	20 min	113 ± 67	988 ± 139***	423 ± 76***/$^{\#\#\#}$	367 ± 58***/$^{\#\#\#}$	195 ± 16$^{\#\#\#}$
C_{max} (ng/mL)		590.2 ± 261.0	4544 ± 506	2129 ± 361	1693 ± 280	1015 ± 73
T_{max} (min)		13 ± 6	11 ± 3	7 ± 3	9 ± 4	≤5
C_{brain} (ng/g)		102 ± 61	468 ± 98***	133 ± 25 $^{\#\#\#}$	89 ± 40$^{\#\#\#}$	38 ± 9$^{\#\#\#}$
brain-to-plasma ratio		0.256 ± 0.041	0.199 ± 0.027*	0.190 ± 0.028**	0.117 ± 0.025***/$^{\#\#\#}$	0.112 ± 0.011***/$^{\#\#\#}$
fold change		1	0.7	0.7	0.5	0.4
C_{liver} (ng/g)		2420 ± 1479	8178 ± 1380***	2147 ± 551$^{\#\#\#}$	2125 ± 701$^{\#\#\#}$	963.4 ± 207$^{\#\#\#}$
liver-to-plasma ratio		5.06 ± 0.96	2.78 ± 0.19***	2.36 ± 0.67***	1.70 ± 0.34***/$^{\#}$	1.66 ± 0.22***/$^{\#}$
fold change		1	0.5	0.5	0.3	0.3

[a]AUC, area under the plasma concentration−time curve; C_{max} maximum ibrutinib concentration in plasma; T_{max}, the time (min) after drug administration needed to reach maximum plasma concentration; C_{brain}, brain concentration; C_{liver}, liver concentration. *, $p < 0.05$; **, $p < 0.01$; and ***, $p < 0.001$ compared to WT mice and $^{\#}$, $p < 0.05$; $^{\#\#}$, $p < 0.01$; and $^{\#\#\#}$, $p < 0.001$ compared to Cyp3a$^{-/-}$ mice. Data are given as mean ± SD.

Our finding that mAbcb1 deficiency unexpectedly decreased ibrutinib oral bioavailability in our new mouse facility but not in our old facility, may be explained by the concomitant introduction of an entirely new intestinal microflora. For instance, bacterial inducing compounds present in our new microflora, but not the old, might cause upregulation of ibrutinib-metabolizing enzymes. If these inducers are normally kept out of the system by mAbcb1, this would result in higher metabolic clearance and hence lower plasma levels of ibrutinib in Abcb1-deficient mice in the new facility. In this context, it is interesting to note that the ibrutinib-DiOH-to-ibrutinib plasma ratios in the old mouse facility were similar between Abcb1a/1b;Abcg2$^{-/-}$ and WT mice (Figure S3), whereas in the new mouse facility, they were about 2-fold higher in both Abcb1a/1b-deficient strains compared to the WT mice (Figure S4). This would be in line with a relatively more extensive metabolic conversion of ibrutinib to ibrutinib-DiOH in the new mouse facility in the Abcb1a/1b-deficient strains. Needless to say, given the (mostly uncharted) complexity of intestinal microflora composition, the identity of any intestinal inducing compounds would be difficult to resolve.

Our CYP3A studies show that, like in humans, ibrutinib oral bioavailability is strongly restricted by CYP3A-mediated conversion to ibrutinib-DiOH. This is true for both the mouse Cyp3a family (encompassing some 8 functional Cyp3a genes) and the transgenic human CYP3A4. The observation that the endogenous mouse Cyp3a proteins had an even stronger effect on ibrutinib oral bioavailability than the transgenic human CYP3A4 (Figure 4) may reflect effectively higher expression of one or more of the mouse Cyp3a proteins and/or higher intrinsic efficacy in metabolizing ibrutinib. This finding is therefore not in itself surprising. In the CYP3A4 transgenic mice, liver and intestinal expression of CYP3A4 are of the same order as that seen in human liver.[40] Our data on ibrutinib and ibrutinib-DiOH levels in the CYP3A4 transgenic mouse strains therefore suggest that intestinal CYP3A4 is at least as important as hepatic CYP3A4 in limiting ibrutinib oral bioavailability (Tables 2 and S2), most likely through extensive first-pass metabolism. Altogether, it seems likely that the poor oral bioavailability of ibrutinib is in large part due to its extensive first-pass metabolism, primarily by CYP3A. This may well also apply in humans, which show an absolute ibrutinib oral bioavailability of only ∼3−8%.[6,29] Apart from its impact on oral bioavailability, CYP3A activity does not seem to have a substantial effect on the tissue distribution of ibrutinib and ibrutinib-DiOH.

Collectively, our data show that extensive metabolism of ibrutinib by CYP3A in intestine and liver is likely the primary factor in restricting its oral bioavailability, whereas the drug efflux transporters ABCB1 and ABCG2 play very little, if any, role in this process. However, the brain distribution of ibrutinib is clearly limited by ABCB1, whereas the relative distribution of ibrutinib to a range of other tissues is not much affected by either the ABC transporters or CYP3A. Considering that the main types of dose-limiting toxicities of ibrutinib (hemorrhage, opportunistic infections, cytopenia, atrial fibrillation, and hypertension) originate outside the CNS, one could consider co-administering ibrutinib with a pharmacological ABCB1 inhibitor in cases where optimal brain penetration of ibrutinib might be therapeutically helpful. However, such treatment modalities would, as always, first have to be very carefully assessed in human patients to judge their practical applicability.

DOI: 10.1021/acs.molpharmaceut.8b00702
Mol. Pharmaceutics 2018, 15, 5124−5134

■ ASSOCIATED CONTENT

Supporting Information

The Supporting Information is available free of charge on the ACS Publications website at DOI: 10.1021/acs.molpharmaceut.8b00702.

Pharmacokinetic parameters, representation of the formation of ibrutinib-DiOH from ibrutinib, plasma concentration−time curves, concentration ratios, kidney and spleen concentrations, tissue-to-plasma ratios, and relative tissue accumulation (PDF)

■ AUTHOR INFORMATION

Corresponding Author

*Phone: +31 20 512 2046; E-mail: a.schinkel@nki.nl.

ORCID

Stéphanie van Hoppe: 0000-0001-9094-5814

Notes

The authors declare the following competing financial interest(s): The research group of A.H.S. receives revenue from commercial distribution of some of the mouse strains used in this study. The other authors declare no conflicts of interest.

■ REFERENCES

(1) Schinkel, A. H.; Wagenaar, E.; Mol, C. A.; van Deemter, L. P-glycoprotein in the blood-brain barrier of mice influences the brain penetration and pharmacological activity of many drugs. *J. Clin. Invest.* **1996**, *97* (11), 2517−2524.

(2) Vlaming, M. L.; Lagas, J. S.; Schinkel, A. H. Physiological and pharmacological roles of ABCG2 (BCRP): recent findings in Abcg2 knockout mice. *Adv. Drug Delivery Rev.* **2009**, *61* (1), 14−25.

(3) Yabuki, N.; Sakata, K.; Yamasaki, T.; Terashima, H.; Mio, T.; Miyazaki, Y.; Fujii, T.; Kitada, K. Gene amplification and expression in lung cancer cells with acquired paclitaxel resistance. *Cancer Genet. Cytogenet.* **2007**, *173* (1), 1−9.

(4) van Hoppe, S.; Sparidans, R. W.; Wagenaar, E.; Beijnen, J. H.; Schinkel, A. H. Breast cancer resistance protein (BCRP/ABCG2) and P-glycoprotein (P-gp/ABCB1) transport afatinib and restrict its oral availability and brain accumulation. *Pharmacol. Res.* **2017**, *120*, 43−50.

(5) Stuurman, F. E.; Nuijen, B.; Beijnen, J. H.; Schellens, J. H. M. Oral anticancer drugs: mechanisms of low bioavailability and strategies for improvement. *Clin. Pharmacokinet.* **2013**, *52* (6), 399−414.

(6) *Center for Drug valuation and Research of the U.S., Department of Health and Human Services Food and Drug Administration*; 2017, https://www.accessdata.fda.gov/drugsatfda_docs/label/2017/205552s017lbl.pdf.

(7) Masso-Valles, D.; et al. Ibrutinib exerts potent antifibrotic and antitumor activities in mouse models of pancreatic adenocarcinoma. *Cancer Res.* **2015**, *75* (8), 1675−1681.

(8) Rauf, F.; Festa, F.; Park, J. G.; Magee, M.; Eaton, S.; Rinaldi, C.; Betanzos, C. M.; Gonzalez-Malerva, L.; LaBaer, J. Ibrutinib inhibition of ERBB4 reduces cell growth in a WNT5A-dependent manner. *Oncogene* **2018**, *37*, 2237.

(9) Sagiv-Barfi, I.; Kohrt, H. E. K.; Czerwinski, D. K.; Ng, P. P.; Chang, B. Y.; Levy, R. Therapeutic antitumor immunity by checkpoint blockade is enhanced by ibrutinib, an inhibitor of both BTK and ITK. *Proc. Natl. Acad. Sci. U. S. A.* **2015**, *112* (9), E966−72.

(10) Berglof, A.; Hamasy, A.; Meinke, S.; Palma, M.; Krstic, A.; Mansson, R.; Kimby, E.; Osterborg, A.; Smith, C. I. E. Targets for Ibrutinib Beyond B Cell Malignancies. *Scand J. Immunol* **2015**, *82* (3), 208−217.

(11) Busygina, K.; Jamasbi, J.; Seiler, T.; Deckmyn, H.; Weber, C.; Brandl, R.; Lorenz, R.; Siess, W. Oral Bruton tyrosine kinase inhibitors selectively block atherosclerotic plaque-triggered thrombus formation. *Blood* **2018**, *131*, 2605.

(12) Honigberg, L. A.; et al. The Bruton tyrosine kinase inhibitor PCI-32765 blocks B-cell activation and is efficacious in models of autoimmune disease and B-cell malignancy. *Proc. Natl. Acad. Sci. U. S. A.* **2010**, *107* (29), 13075−80.

(13) Wang, X.; Wong, J.; Sevinsky, C. J.; Kokabee, L.; Khan, F.; Sun, Y.; Conklin, D. S. Bruton's Tyrosine Kinase Inhibitors Prevent Therapeutic Escape in Breast Cancer Cells. *Mol. Cancer Ther.* **2016**, *15* (9), 2198−2208.

(14) Zhang, H.; et al. The BTK Inhibitor Ibrutinib (PCI-32765) Overcomes Paclitaxel Resistance in ABCB1- and ABCC10-Overexpressing Cells and Tumors. *Mol. Cancer Ther.* **2017**, *16* (6), 1021−1030.

(15) Scheers, E.; et al. Absorption, metabolism, and excretion of oral (1)(4)C radiolabeled ibrutinib: an open-label, phase I, single-dose study in healthy men. *Drug Metab. Dispos.* **2015**, *43* (2), 289−297.

(16) *Center for Drug valuation and Research of the U.S., Department of Health and Human Services Food and Drug Administration, 203469Orig1s000*; 2012, http://www.accessdata.fda.gov/drugsatfda_docs/nda/2012/203469Orig1s000ClinPharmR.pdf.

(17) *Novartis Pharmaceuticals Corporation, Gleevec*; 2004, https://www.pharma.us.novartis.com/sites/www.pharma.us.novartis.com/files/gleevec_tabs.pdf.

(18) *Novartis Pharmaceuticals, Tasigna [package insert]*; 2014, https://www.pharma.us.novartis.com/product/pi/pdf/tasigna.pdf.

(19) Li, X.; He, Y.; Ruiz, C. H.; Koenig, M.; Cameron, M. D. Characterization of dasatinib and its structural analogs as CYP3A4 mechanism-based inactivators and the proposed bioactivation pathways. *Drug Metab. Dispos.* **2009**, *37* (6), 1242−1250.

(20) Abbas, R.; Hug, B. A.; Leister, C.; Burns, J.; Sonnichsen, D. Effect of ketoconazole on the pharmacokinetics of oral bosutinib in healthy subjects. *J. Clin. Pharmacol.* **2011**, *51* (12), 1721−1727.

(21) Rood, J. J.; Van Hoppe, S.; Schinkel, A. H.; Schellens, J. H. M.; Beijnen, J. H.; Sparidans, R. W. Liquid chromatography-tandem mass spectrometric assay for the simultaneous determination of the irreversible BTK inhibitor ibrutinib and its dihydrodiol-metabolite in plasma and its application in mouse pharmacokinetic studies. *J. Pharm. Biomed. Anal.* **2016**, *118*, 123−131.

(22) Durmus, S.; Sparidans, R. W.; Wagenaar, E.; Beijnen, J. H.; Schinkel, A. H. Oral availability and brain penetration of the B-RAFV600E inhibitor vemurafenib can be enhanced by the P-GLYCOprotein (ABCB1) and breast cancer resistance protein (ABCG2) inhibitor elacridar. *Mol. Pharmaceutics* **2012**, *9* (11), 3236−3245.

(23) Schinkel, A. H.; et al. Normal viability and altered pharmacokinetics in mice lacking mdr1-type (drug-transporting) P-glycoproteins. *Proc. Natl. Acad. Sci. U. S. A.* **1997**, *94* (8), 4028−4033.

(24) Jonker, J. W.; et al. The breast cancer resistance protein protects against a major chlorophyll-derived dietary phototoxin and protoporphyria. *Proc. Natl. Acad. Sci. U. S. A.* **2002**, *99* (24), 15649−15654.

(25) Jonker, J. W.; et al. The breast cancer resistance protein BCRP (ABCG2) concentrates drugs and carcinogenic xenotoxins into milk. *Nat. Med.* **2005**, *11* (2), 127−129.

(26) van Waterschoot, R. A.; et al. Absence of both cytochrome P450 3A and P-glycoprotein dramatically increases docetaxel oral bioavailability and risk of intestinal toxicity. *Cancer Res.* **2009**, *69* (23), 8996−9002.

(27) Dai, H.; et al. Distribution of STI-571 to the brain is limited by P-glycoprotein-mediated efflux. *J. Pharmacol. Exp. Ther.* **2002**, *304* (3), 1085−1092.

(28) Goh, L. B.; Spears, K. J.; Yao, D.; Ayrton, A.; Morgan, P.; Wolf, R. C.; Friedberg, T. Endogenous drug transporters in in vitro and in vivo models for the prediction of drug disposition in man. *Biochem. Pharmacol.* **2002**, *64* (11), 1569−1578.

(29) *European Medicines Agency*; 2014, http://www.ema.europa.eu/docs/en_GB/document_library/EPAR_-_Product_Information/human/003791/WC500177775.pdf.

DOI: 10.1021/acs.molpharmaceut.8b00702
Mol. Pharmaceutics 2018, 15, 5124−5134

(30) Bernard, S.; et al. Activity of ibrutinib in mantle cell lymphoma patients with central nervous system relapse. *Blood* **2015**, *126* (14), 1695−1698.
(31) Boudin, L.; Patient, M.; Romeo, E.; Blade, J.-S.; de Jaureguiberry, J.-P. Efficacy of ibrutinib as first-line treatment of tumoral Bing-Neel syndrome. *Leuk. Lymphoma* **2018**, 1−3.
(32) Lionakis, M. S.; et al. Inhibition of B Cell Receptor Signaling by Ibrutinib in Primary CNS Lymphoma. *Cancer Cell* **2017**, *31* (6), 833.
(33) Mason, C.; et al. Ibrutinib penetrates the blood brain barrier and shows efficacy in the therapy of Bing Neel syndrome. *Br. J. Haematol.* **2017**, *179* (2), 339−341.
(34) Hiemcke-Jiwa, L. S.; et al. Efficacy of ibrutinib in a patient with transformed lymphoplasmacytic lymphoma and central nervous system involvement. *Leuk. Lymphoma* **2018**, *59* (5), 1256−1259.
(35) Uchida, Y.; et al. Quantitative targeted absolute proteomics of human blood-brain barrier transporters and receptors. *J. Neurochem.* **2011**, *117* (2), 333−345.
(36) Drean, A.; et al. ATP binding cassette (ABC) transporters: expression and clinical value in glioblastoma. *J. Neuro-Oncol.* **2018**, *138* (3), 479−486.
(37) Olarte Carrillo, I.; et al. Clinical significance of the ABCB1 and ABCG2 gene expression levels in acute lymphoblastic leukemia. *Hematology* **2017**, *22* (5), 286−291.
(38) Kort, A.; et al. Brain and Testis Accumulation of Regorafenib is Restricted by Breast Cancer Resistance Protein (BCRP/ABCG2) and P-glycoprotein (P-GP/ABCB1). *Pharm. Res.* **2015**, *32* (7), 2205−2216.
(39) Kort, A.; et al. Brain Accumulation of Ponatinib and Its Active Metabolite, N-Desmethyl Ponatinib, Is Limited by P-Glycoprotein (P-GP/ABCB1) and Breast Cancer Resistance Protein (BCRP/ABCG2). *Mol. Pharmaceutics* **2017**, *14* (10), 3258−3268.
(40) van Herwaarden, A. E.; et al. Knockout of cytochrome P450 3A yields new mouse models for understanding xenobiotic metabolism. *J. Clin. Invest.* **2007**, *117* (11), 3583−3592.

DOI: 10.1021/acs.molpharmaceut.8b00702
Mol. Pharmaceutics 2018, 15, 5124−5134